PNAS RESEARCH ARTICLE | ENVIRONMENTAL SCIENCES ANTHROPOLOGY OPEN ACCESS

Ice and ocean constraints on early human migrations into North America along the Pacific coast

Summer K. Praetorius[a,1], Jay R. Alder[b], Alan Condron[c], Alan C. Mix[d], Maureen H. Walczak[d], Beth E. Caissie[a,e], and Jon M. Erlandson[f]

Edited by Cathy Whitlock, Montana State University Bozeman, Bozeman, MT; received May 24, 2022; accepted December 19, 2022

Founding populations of the first Americans likely occupied parts of Beringia during the Last Glacial Maximum (LGM). The timing, pathways, and modes of their southward transit remain unknown, but blockage of the interior route by North American ice sheets between ~26 and 14 cal kyr BP (ka) favors a coastal route during this period. Using models and paleoceanographic data from the North Pacific, we identify climatically favorable intervals when humans could have plausibly traversed the Cordilleran coastal corridor during the terminal Pleistocene. Model simulations suggest that northward coastal currents strengthened during the LGM and at times of enhanced freshwater input, making southward transit by boat more difficult. Repeated Cordilleran glacial-calving events would have further challenged coastal transit on land and at sea. Following these events, ice-free coastal areas opened and seasonal sea ice was present along the Alaskan margin until at least 15 ka. Given evidence for humans south of the ice sheets by 16 ka and possibly earlier, we posit that early people may have taken advantage of winter sea ice that connected islands and coastal refugia. Marine ice-edge habitats offer a rich food supply and traversing coastal sea ice could have mitigated the difficulty of traveling southward in watercraft or on land over glaciers. We identify 24.5 to 22 ka and 16.4 to 14.8 ka as environmentally favorable time periods for coastal migration, when climate conditions provided both winter sea ice and ice-free summer conditions that facilitated year-round marine resource diversity and multiple modes of mobility along the North Pacific coast.

paleoceanography | sea ice | human migration | North Pacific | paleoclimate

Significance

Growing evidence for a human presence in the Americas prior to 15,000 y ago—when ice sheets blocked transit through the continental interior—imply a Pacific Coast route was the more likely pathway for dispersals from Beringia into North America between ~26,000 and 14,000 y ago. The feasibility of coastal migration at various times depended on the extent of Cordilleran glaciers, sea ice, the strength of ocean currents, and the productivity and availability of marine and terrestrial resources. Based on paleoclimate records and climate models, we estimate that 24,500 to 22,000 and 16,400 to 14,800 y ago were the most environmentally favorable time windows for a coastal migration during the period when the interior route was blocked.

Human dispersal pathways from Beringia into North America continue to be debated. Prevailing ideas include a coastal route and an interior route via an ice-free corridor between the Laurentide and Cordilleran ice sheets (1–6). The Laurentide and Cordilleran ice sheets merged during the Last Glacial Maximum (LGM) (7), closing the ice-free inland corridor between ~26 ± 1 ka (Fig. 1 and ref. 8) and 13.8 ± 0.5 ka (ref. 9). Archaeological sites south of the ice sheets in North America during this time frame (10–15) thus require either a coastal route, or entry through the interior prior to the LGM. A pre-LGM migration scenario is at odds with apparent genetic divergence between Siberian and Beringian populations between about 25 to 24 ka (95% CI 21 to 28 ka; ref. 16) and an inferred "Beringian Standstill" in migration until 18 to 16 ka (16–19). Was this biogeographical pause due to favorable conditions in Beringia, glacial bottlenecks that prevented southward transit along the coast, or a combination of both? How did Beringians make the arduous journey along the Pacific Coast corridor – by land, sea, or ice? Was the coastal route effectively blocked throughout the LGM, or were there intervals when passage was more or less possible? Building on recent evidence for multiple intervals of Cordilleran ice retreat within the last ice age (20), we evaluate these scenarios and define relatively benign climatic intervals when human migration along the Cordilleran coast may have been most feasible.

Despite evidence for older archaeological sites farther inland, thus far, there is no definitive evidence of human occupation along the Pacific Coast of North America prior to ~13.8 ka (23). The absence of earlier coastal sites may reflect submergence of former occupation sites by rising postglacial sea level, exacerbated locally by relaxation of a subsiding glacio-isostatic forebulge (3, 24). Other factors may also have limited the viability of a coastal transit at certain times. The most obvious obstacle is ice cover on land, with large outlet glaciers emanating from the Alaska Peninsula and Southeast Alaska terminating in the ocean. Heavily crevassed ice streams would have been difficult or impossible to cross on land and dangerous at sea, potentially preventing passage for migrating groups of people.

The strength of the cyclonic Alaska Coastal Current (ACC) also may have partially impeded southward movement for seafarers, as this current flows northward against the direction of migration (25). The ACC is driven by wind and Coriolis forcing and strengthened by coastal freshwater inputs (26) (Fig. 2). Royer and Finney (25) hypothesized that southward migration was impeded by freshwater input and rapid sea-level rise that accelerated coastal currents during global Meltwater Pulse 1a (MWP1a: 14.65 to 14.30

Author affiliations: [a]U.S. Geological Survey, Menlo Park, CA 94025; [b]U.S. Geological Survey, Corvallis, OR 97331; [c]Woods Hole Oceanographic Institution, Woods Hole, MA 02543; [d]Oregon State University, Corvallis, OR 97331; [e]University of California, Santa Cruz, CA 95064; and [f]University of Oregon, Eugene, OR 97403

Author contributions: S.K.P. designed research; S.K.P., J.R.A., A.C. performed research; S.K.P., J.R.A., A.C., A.C.M contributed new reagents/analytic tools; S.K.P., J.R.A., A.C., A.C.M, M.H.W., B.E.C., J.M.E. analyzed data; and S.K.P., J.R.A., A.C., A.C.M, B.E.C., J.M.E. wrote the paper.

The authors declare no competing interest.

This article is a PNAS Direct Submission.

[1]To whom correspondence may be addressed. Email: spraetorius@usgs.gov.

This article contains supporting information online at https://www.pnas.org/lookup/suppl/doi:10.1073/pnas.2208738120/-/DCSupplemental.

Published February 6, 2023.

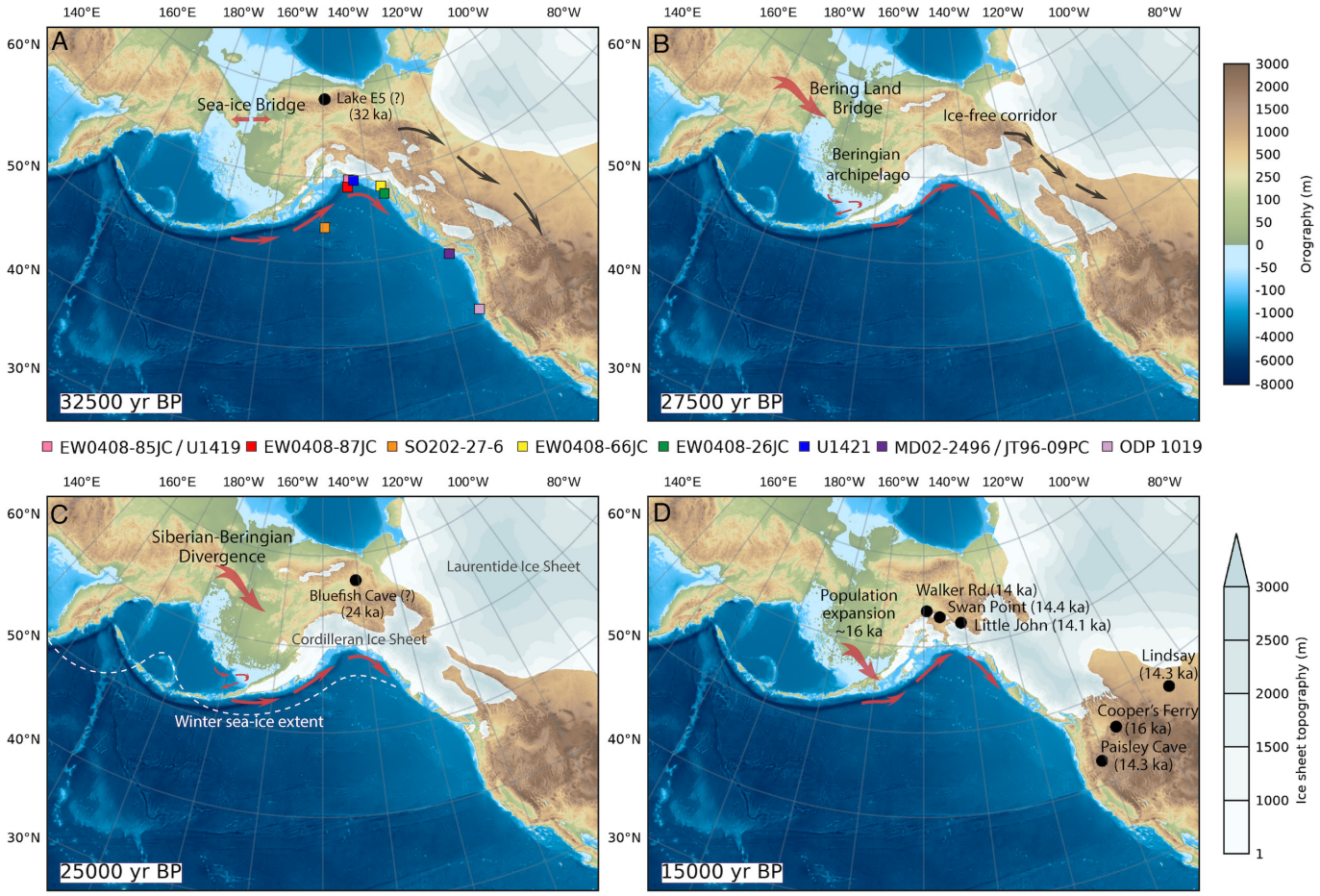

Fig. 1. Map of coastlines and ice extent at various time periods A) 32.5 ka, B) 27.5 ka, C) 25 ka, D) 15 ka during the late Pleistocene, showing possible migration pathways at each stage. Relative sea level (RSL) and ice sheet topography are from (8) and are interpolated and applied to the ETOPO01 bathymetry grid (21). Post LGM glacial ice evolution is unknown for Siberia, though some ice sheets were likely present during these time periods. North American archaeological sites (black dots) are shown that have median dates for initial human occupation that fall within ± 1 ka of the various time slices shown (for a full list of archaeological site data and references, including those that fall outside of the time/space domains shown here, see *SI Appendix,* Table S1 and Dataset S1); sites with controversial evidence for human presence are denoted with question marks. White dashed line on panel (*C*) shows the estimated extent of winter sea ice during the LGM, based on (22). Seasonal sea ice was present along the Alaskan coastal corridor to varying degrees during all the periods shown, but the spatial extent is not as well defined for the other intervals. Sediment cores identified in panel (*A*) are for the various proxy datasets shown in Figs. 3 and 5.

ka; ref. 27), effectively assuming that local freshwater inputs tracked global-average sea-level rise. Testing this hypothesis requires reconstruction of regional ice retreat and the resulting reduction of coastal salinity from regional meltwater flux, along with quantitative modeling of coastal current strength, issues we address here.

The extent of land ice, both along the coastal corridor and inland route, has been widely debated over many decades (4, 28–30). However, the assessment of ice in the marine environment—such as the extent of sea ice and icebergs, and their impact on human migration—has received less attention. Evidence from ice-rafted debris (IRD) in marine sediments shows that the seaward edge of the Cordilleran Ice Sheet (CIS) and its outlet glaciers was extremely variable and subject to repeated abrupt retreats onto land or into silled fjords during the late Pleistocene (referred to as "Siku Events"; ref. 20). Sea ice formed in the subarctic North Pacific through much of this interval (22, 31), which may have impacted boat transit and altered marine resource composition and availability during certain months of the year. Today, land-fast sea ice provides a relatively unobstructed and flat surface as a platform for travel between otherwise inaccessible high Arctic communities, typically in winter or spring (32, 33). In addition to ease of movement, sea ice facilitates hunting of marine mammals near the ice edge and sub-ice intertidal shellfishing; both are important food resources in the Arctic winter (32). With the seasonal melting of sea ice, kelp forest habitats can provide important marine resources in summer (34, 35). Reconstructions of North Pacific sea ice are essential to building a clearer picture of the conditions that coastal people in the North Pacific would have contended with during the glacial and deglacial periods.

To help address these issues, we present records of sea-ice variations based on the $\%C_{37:4}$ proxy (36) and synthesize previously published reconstructions of sea ice, sea-surface temperature (SST), salinity, and IRD from marine sediment cores in the North Pacific (Fig. 1). Together, these paleoenvironmental data help discern major climate and oceanographic changes that may have facilitated or impeded human migration during the terminal Pleistocene. We present model results from a high-resolution (1/6°) eddy-permitting general circulation model (MITgcm) and a lower resolution model (GENMOM) to evaluate changes in current velocity of the Alaska Current system between glacial and modern climate states, as well as in response to increases in regional freshwater discharges and intermediate sea level conditions. We compare paleo-SST reconstructions from the North Pacific with simulated SST from the transient deglacial simulation in iTRACE (37) for major climate intervals between the LGM and early Holocene. These paleoenvironmental reconstructions and models suggest possible time

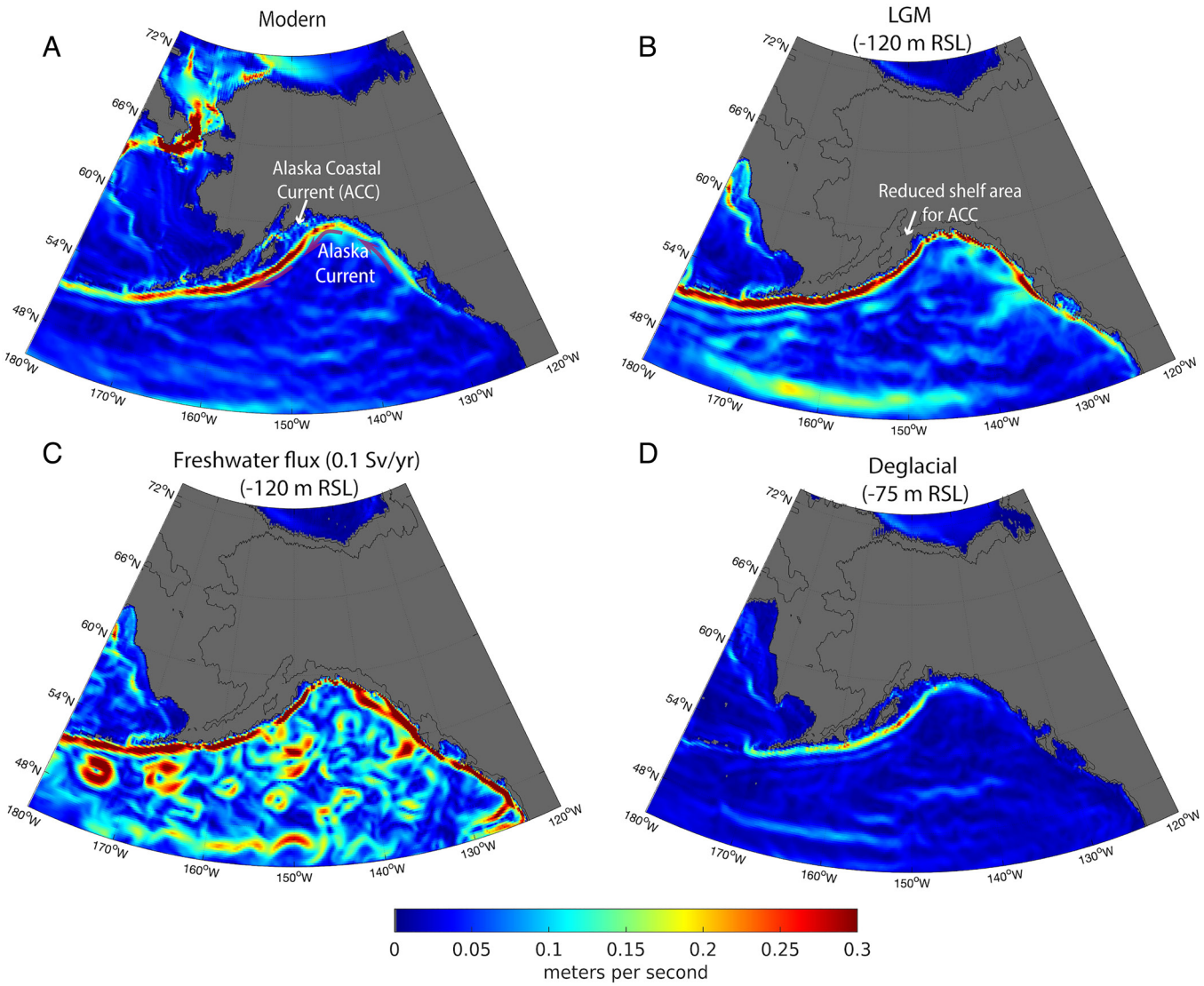

Fig. 2. Simulations of ocean currents in the Northeast Pacific under different climate and sea level conditions: Modern climate state (*A*), LGM climate state, with sea level −120 m below modern (*B*), LGM boundary conditions with an increased freshwater flux (*C*), and intermediate sea level (−75 m), as would have occurred during the mid-deglacial period (*D*). Mean annual surface ocean velocity shows a strengthening of the cyclonic Alaska Current during the LGM relative to modern conditions, as well as a contraction of the shelf area on which the ACC flows. Boundary currents flow in a cyclonic (anticlockwise) direction.

intervals when southward dispersal along the Northwest Coast was most feasible for people and provide insight into factors that may have influenced subsequent coastal habitability.

Results

Ocean Currents. The Alaska, Kuroshio, Kamchatka, and Oyashio Currents all increased their velocities during the LGM simulation relative to the modern (Fig. 2 *A* and *B* and *SI Appendix,* Figs. S1 and S2) reflecting stronger ice-age wind forcing driven by greater meridional temperature gradients (38). The strengthening of the northward flowing Alaska currents during the LGM is contrary to the weaker glacial currents previously hypothesized (25). Our simulation shows that lower LGM sea levels restricted the shelf area over which the modern Alaskan Coastal Current (ACC) flows, thus the geostrophic currents were focused into a single high-velocity stream that flowed along the Alaskan margin.

Simulations in which various freshwater fluxes [0.05 to 3.0 Sv (10^6 m^3 s^{-1})] are discharged into the North Pacific Ocean via the Columbia River over the course of a year result in an increase in the velocity of the Alaska Current (Fig. 2*C* and *SI Appendix,* Figs. S3 and S4). These simulations mimic a range of transient floods of freshwater caused by glacial outburst floods (39) but can be used to approximate the impacts of increased freshwater fluxes on regional current speeds, such as would have come from a range of sources and discharge locations along the Cordilleran margin, including iceberg discharge. Changes in current velocity are most sensitive to the lower range of meltwater volumes, such that the percentage increase in velocity rises more steeply (~three times) in response to smaller fluxes (0.05 to 0.5 Sv) than to the largest additions of meltwater (*SI Appendix,* Fig. S4). Our simulations support the idea that enhanced freshwater flux increases the strength of the Alaska Current (25), but regional paleosalinity reconstructions indicate that the early deglacial period (~18.5 to 16.0 ka) was the time of maximum surface freshening (40–42), rather than 14.65 to 14.30 ka as previously assumed (25). The older interval coincides with peak deposition of IRD in the Gulf of Alaska (20, 42) and large Missoula Flood events from the Columbia River (43).

To assess impacts of sustained meltwater over longer time periods, we also ran multicentennial simulations in the lower resolution-coupled atmosphere-ocean GCM GENMOM (*Methods*), with sustained meltwater fluxes of 0.02 to 0.05 Sv applied along the Cordilleran

coast, as may have occurred during a Siku Event. These simulations show decreases in surface salinity, SST, and air temperatures in the Northeast Pacific, as well as an attendant increase in ocean current speeds in the Gulf of Alaska (*SI Appendix*, Figs. S5 and S6).

A high-resolution simulation with intermediate sea levels (−75 m) run under modern climate forcing resulted in weaker current strengths than under the LGM or modern configuration (Fig. 2*D*). This supports the idea that coastal currents would have been attenuated as sea level transgressed across the continental shelf (25), in the absence of changes in wind forcing. Intermediate sea levels would have occurred during the middle of the deglaciation, for example during the Bølling-Allerød warm interval (14.7 to 12.9 ka), when dust fluxes in Greenland were low (44), indicating weaker winds than during the LGM.

Sea-Ice Reconstructions. We assess sea-ice reconstructions from the Gulf of Alaska between 54.2 and 59.6°N based on various sea-ice proxies, including the IP_{25} index, sea-ice diatom assemblages, and the relative abundance of the C_{37} tetra-unsaturated methyl alkenone ($\%C_{37:4}$) (Fig. 3). Our records of $\%C_{37:4}$ show maximum sea ice abundance between 18.0 and 16.5 ka, concurrent with cool Northeast Pacific SSTs (Fig. 3). The most abundant and seasonally persistent sea ice probably occurred close to the continental margin in the northernmost Gulf of Alaska (core EW0408-85JC), given the higher $\%C_{37:4}$ at this site relative to others. The $\%C_{37:4}$ declined steadily after 17 ka, followed by a brief resurgence around 15.7 ka. $\%C_{37:4}$ is low (~5%) between ~14.8 and 13 ka (roughly coeval with the Bølling-Allerød interval), but some winter sea ice was likely present based on the occurrence of sea-ice diatoms in marine sediments (42, 45). The relative abundance of $C_{37:4}$ increases to above 10% during the Younger Dryas period (~13 to 12 ka), indicating an increase in winter sea ice during this cold period at sites in the northernmost Gulf of Alaska.

These data confirm and improve on previous chronologies of sea ice based on the IP_{25} index, sea-ice diatoms, and dinocyst assemblages in the North Pacific and Bering Sea (22, 31, 42, 45–47). Collectively, these multiproxy records indicate that winter sea ice was extensive and persistent in the Bering Sea and Gulf of Alaska between ~26 and 15 ka and was present intermittently in the Gulf of Alaska during late Marine Isotope Stage 3 (42 to 27 ka). Sea ice was likely present but of restricted extent during the Bølling–Allerød warm period (~14.8 to 13.0 ka), expanded during the Younger Dryas (~13 to 12 ka), and then disappeared from the Gulf of Alaska entirely by the early Holocene (~11 ka).

It is likely that sea ice was present in winter but mostly melted during summer in the Gulf of Alaska, even during the last glacial interval. Values of $\%C_{37:4}$ between ~10 and 50% in the Gulf of Alaska records during the LGM and early deglacial period would correspond to ~20 to 60% mean annual sea ice concentrations based on modern observed correlations (36), indicating sea ice was present during only the coldest months of the year, and the IP_{25}, diatom-, and dinocyst-based sea ice records show no indication of perennial sea ice during these times (22, 31, 45–47). SST reconstructions from the Bering Sea and Gulf of Alaska also indicate ocean temperatures remained above freezing during summer months throughout the LGM, implying that extensive winter sea ice would have given way to open water conditions during summer (22, 31). These data suggest that seasonal fluctuations between winter sea ice and summer kelp forest and other near-shore habitats persisted for millennia around the margins of the North Pacific, both conditions to which successful coastal people would have had to adapt.

North Pacific SST Variability. Late LGM SSTs (23 to 19 ka) were on average ~2 to 5 °C colder than the early Holocene (11.5 to 10 ka) across much of the North Pacific (Fig. 4), with greatest cooling in the central and eastern North Pacific and less cooling in the Northwest Pacific. Some sites in the western Bering Sea and Sea of Okhotsk yield SST anomalies for the LGM that appear warmer than the early Holocene; however, many of these warm temperatures have been attributed to a strong seasonal bias imposed by prolonged sea-ice cover (48), and anomalously warm $U^{K'}_{37}$ values have been observed in some high-latitude regions (36, 49), so the fidelity of these warm glacial SSTs as representative of mean state changes remains in question.

The interval that encompasses Siku Event 1 (18.0 to 16.5 ka, ref. 20) cooled 0.5 to 2.0 °C relative to the late LGM (23 to 19 ka) at many sites in the North Pacific, reflecting the coldest conditions of the last ~20 ka (Figs. 3 and 4). Warming of 0.5 to 2.0 °C commenced between 16.4 and 14.8 ka across much of the North Pacific. This period was associated with retreat of land ice along the Aleutian Islands and Southeast Alaskan coastline (28, 30, 50, 51), the establishment of postglacial terrestrial vegetation on the Aleutian Islands (50, 51), and conifer forests in Southeast Alaska (52). An episode of abrupt and intensified ocean warming occurred at ~14.8 ka, during the transition into the Bølling–Allerød period. This warming tracked the final retreat of coastal glaciers out of the ocean (53), and a sudden transition to severe subsurface hypoxia, indicating a strengthening and vertical expansion of the North Pacific oxygen minimum zone (53–55). The Younger Dryas saw a return to a cooler ocean, more sea ice, and less hypoxia. The subsequent transition into the Holocene brought another episode of abrupt ocean warming, accompanied by a second ocean hypoxic event (53–55). The hypoxic events were associated with increases in primary productivity and carbon export (53), but it remains unclear how these changes in productivity and ocean oxygen content affected nearshore ecosystems, and whether that in turn could have affected coastal habitability (see *SI Appendix* for further discussion).

Discussion: Paleoclimatic Implications for Human Migrations

We have documented substantial variability in marine and coastal environments within the Alaskan portion of the Pacific Coast Route. Here, we discuss the implications of these environmental reconstructions for identifying the most feasible times of human migration southward into North America.

Glacial Beringia. Our data compilation shows colder SSTs during the late LGM than the early Holocene for much of the North Pacific and Bering Sea, challenging previous notions of anomalous warmth in the subpolar gyre during the LGM (56), with sea-ice reconstructions that indicate extensive seasonal sea ice throughout the subarctic North Pacific (22, 31, 46). While coastal areas in Beringia may have experienced mild, mesic climate in the long days of summer months, the greater continentality of northern Beringia would have led to a drier, colder winter climate, especially inland (57, 58). For example, Löfverström & Liakka (59) attribute the lack of glacial advance in northern Alaska to moisture starvation from a southward shift in the Pacific storm track, whereas mild summer temperatures (comparable to preindustrial) are attributed to an increase in shortwave radiation at the surface due to decreased cloudiness. Model LGM temperature estimates derived from data assimilation show strong annual ocean cooling across the North Pacific gyre, with comparatively modest cooling in Beringia relative to late Holocene temperatures (60). Collectively, these records imply that while Beringia likely experienced net glacial

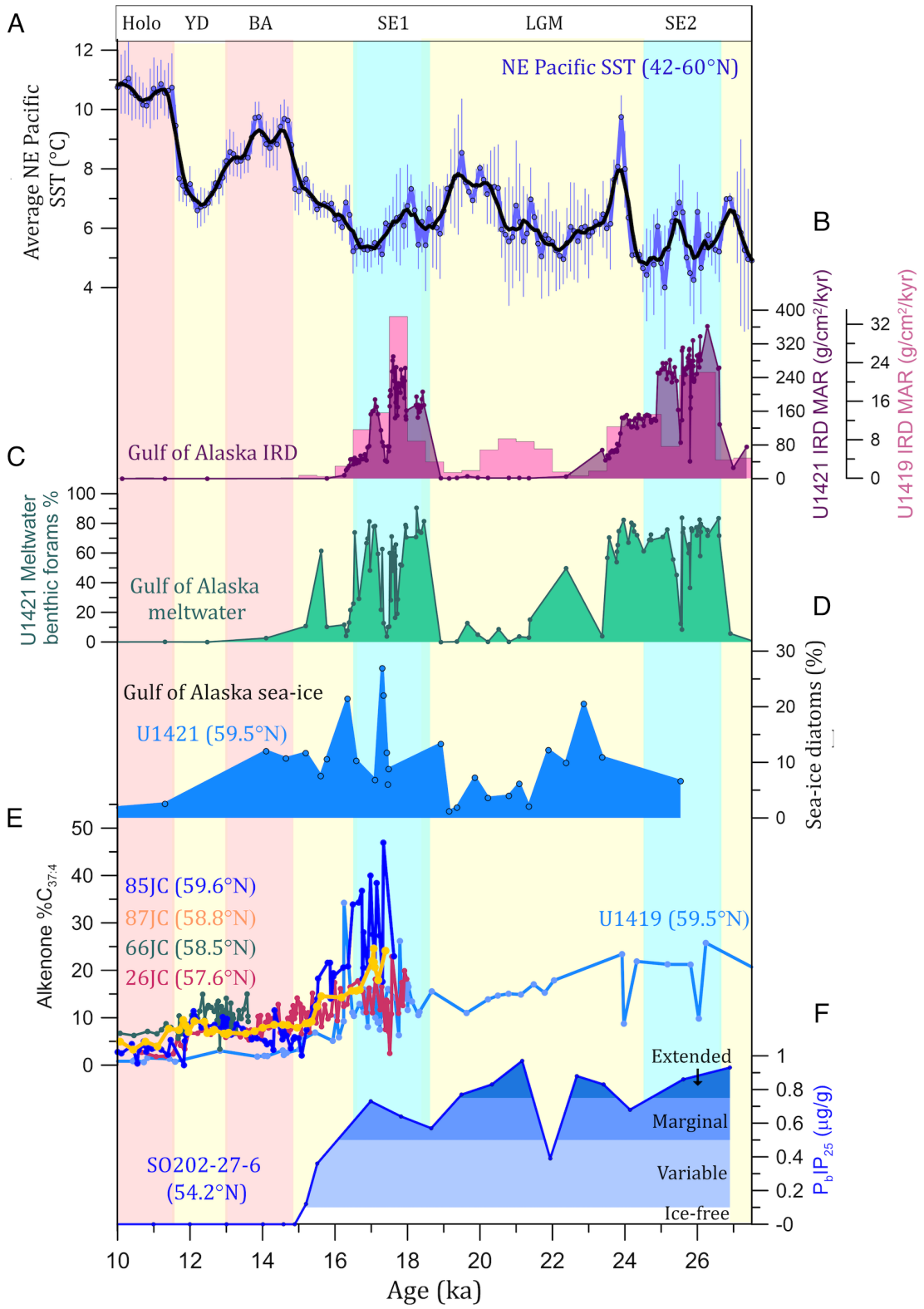

Fig. 3. Northeast Pacific paleoclimate reconstructions from the LGM to early Holocene. (*A*) Average Northeast Pacific SST stack (see *Materials & Methods* and *SI Appendix*, Fig. S7 for details); (*B*) Mass accumulation rate as a proxy of IRD from sites U1421 (dark pink: ref. 42) and U1419 (light pink: ref. 20) in the Gulf of Alaska; (*C*) Percent benthic foraminifera indicative of meltwater from site U1421 (42); (*D*) Percent of sea-ice diatoms in core U1421 (42); (*E*) Alkenone $\%C_{37:4}$ records from various Gulf of Alaska cores as a proxy for sea ice: data from U1419 are from ref. 31, all other data are from this paper; (*F*) $PbIP_{25}$ sea-ice index from site SO202-27-6 in the Gulf of Alaska (22); >0.75 = extended sea ice, 0.5 to 0.75 = marginal sea ice, 0.1 to 0.5 = variable sea ice <0.1 = ice free). Blue shaded bars indicate Siku Events (SE1 & SE2); pink shaded bars indicate warm periods with little sea ice (Bølling-Allerød and early Holocene); yellow shaded bars indicate the inter-Siku time intervals in which winter sea ice was present in the Gulf of Alaska.

cooling relative to Holocene temperatures, it was spared the severe cold of other high-latitude regions, especially during summer months (59).

Short-term climate variability within the full LGM period (26.5 to 19 ka) is not captured in the late LGM SST means (Fig. 4) but can be seen in some high-resolution records. Pronounced

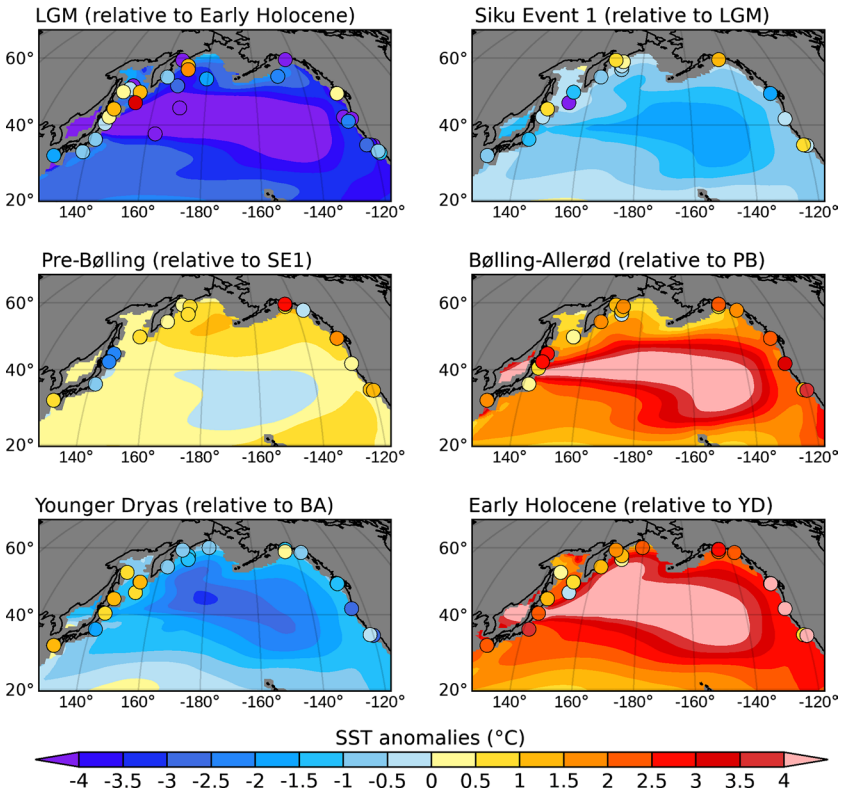

Fig. 4. Annual SST anomalies in the North Pacific for various time periods between the LGM and Holocene. Proxy data anomalies are plotted as dots for specific sites, whereas the interpolated SST fields making up the base maps are from the iTRACE transient simulation (37). The proxy anomalies reflect the following climate intervals: LGM – early Holocene (23.0 to 19.0 ka – 11.5 to 10.0 ka), Siku Event 1 (SE1) – LGM (18.0 to 16.5 ka – 23.0 to 19.0 ka), pre-Bølling (PB) – Siku Event 1 (16.4 to 15.0 ka – 18.0 to 16.5 ka), Bølling-Allerød – pre-Bølling (14.6 to 13.0 ka – 16.4 to 15.0 ka), Younger Dryas (YD) – Bølling-Allerød (12.7 to 12.0 ka – 14.6 to 13.0 ka), early Holocene – YD (11.5 to 10.0 ka – 12.7 to 12.0 ka). The model anomalies follow the same time windows as above, except for the LGM (20.0 to 19.0 ka) and the early Holocene (11.5 to 11.0 ka), which have more restricted time windows due to the length of the transient iTRACE simulation, which spans 20.0 to 11.0 ka.

short-lived warming within the LGM is detected off northern California (ODP Site 1019; refs. 61 and 62) and off the west coast of Vancouver Island (Core MD02-2496; ref. 63) between 24.5 and 24.0 ka (*SI Appendix,* Fig. S7). Acknowledging uncertainties (multicentennial to millennial) in some age models, the overlap in timing between this mid-LGM warming event and genomic estimates for divergence in Siberian and Beringian populations (~25 to 24 ka; refs. 16 and 17) raise the possibility that brief (century-scale) warming events, not yet resolved in most data records, might have provided windows of opportunity for multiple early migrations into Beringia and the Americas.

It has been proposed that humans occupied eastern Beringia continuously between ~32 ka and 19 ka, based on fecal biomarkers (64) (Fig. 1*A*). If so, migration into North America using the interior "Ice-free corridor" could have occurred prior to coalescence of the Laurentide and Cordilleran ice sheets between 27 and 25 ka. However, evidence for such an early migration is contested (65), and no archaeological evidence has been found to corroborate such a human presence in that area (66). Such early migration also conflicts with genomic evidence that Beringian populations were isolated around the beginning of the LGM (16–19). Multiple waves and routes of human dispersal remain possible, with small early populations either dying out or obscured in their genetic contributions (10). Because evidence for a pre-LGM human migration is not widely accepted, we focus on climate constraints for migration intervals that are younger than the closure of the inland ice-free corridor, and within the estimated time frame of Beringian population divergence (<25 ka; ref. 17), while noting that variability of ice cover on land and in the sea, and episodes of climate amelioration, also exist in the interval prior to 25 ka (Fig. 5).

Several North American archaeological sites have produced possible evidence for human occupations during the LGM (10, 15, 69, but see contrary opinions in refs. 70 and 71). These ages are easier to reconcile with the estimated time frames for genetic separation between Siberian and Beringian populations than the purported pre-LGM sites, but still require that humans entered the Americas prior to substantial regional deglaciation. As the interior corridor was ice-filled between ~26 to 14 ka, any migrations that occurred during this period must have followed the Pacific Coast, subject to varying environmental conditions along that pathway that we evaluate here.

Ocean Currents and Migration by Watercraft. Although no firm evidence for Pleistocene-aged boats has been found in Beringia, coastal areas where such activity might be found are now submerged, and the volcanic-rich sediments of the North Pacific generally contribute to poor organic preservation (72). Seafarers in northern Japan were contemporaneous with the earliest Beringian populations, however, so ocean-going watercraft and associated maritime technologies existed in Northeast Asia by at least 35 ka (72, 73).

During the LGM, our model results show that the average strength of the Alaska Current more than doubled along the Southeast Alaska margin relative to modern conditions (Fig. 2*B*). During times of high freshwater input, maximum model current velocities increased to between 0.5 and 2.0 m/s, with chaotic meanders and eddies (Fig. 2*C* and *SI Appendix,* Figs. S3 and S4). These accelerated currents might have impeded southward seafaring migration, and currents during high meltwater events may have been nearly impassable, with peak current velocities that may

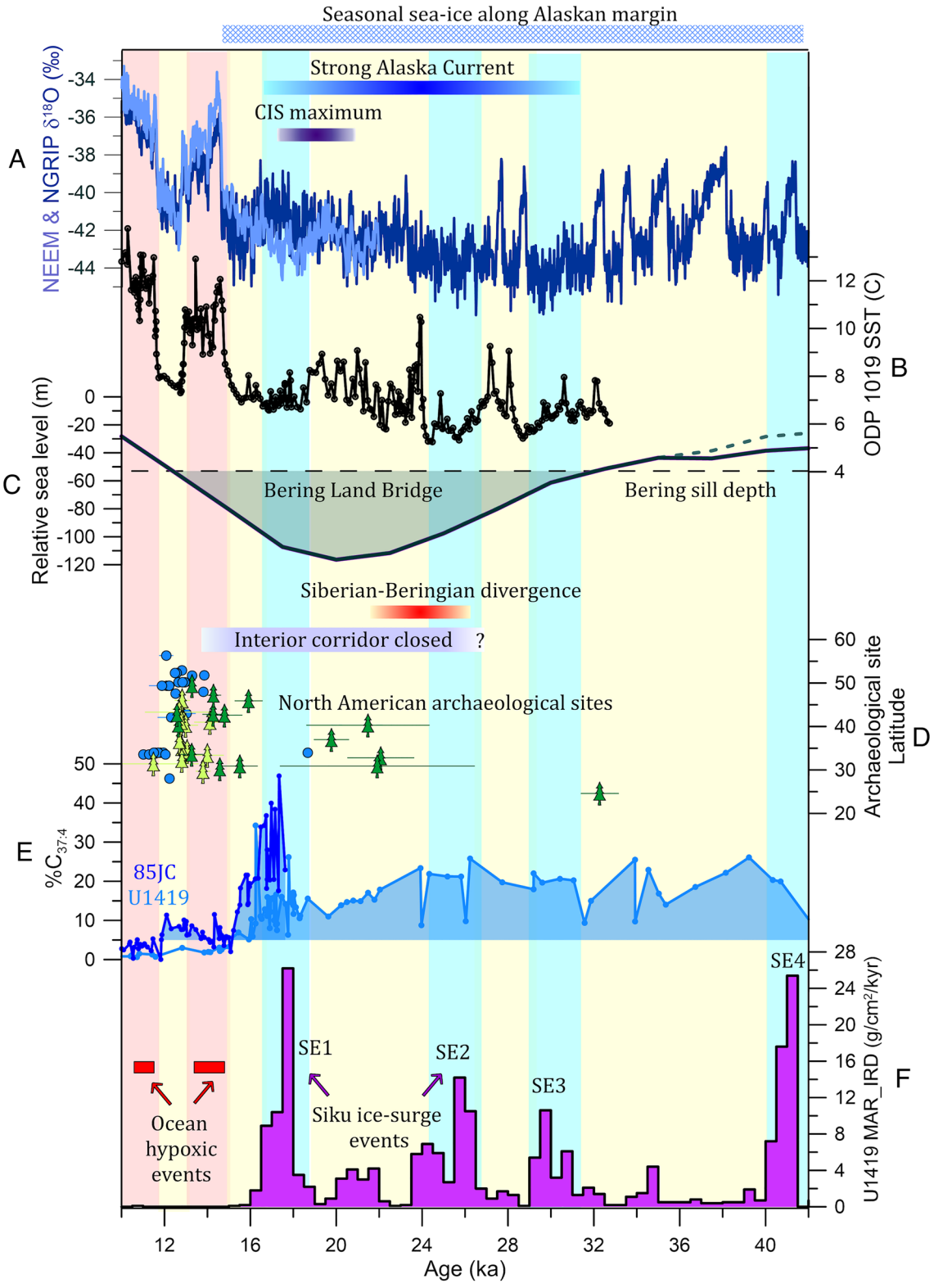

Fig. 5. Timing of abrupt climate change events in the North Pacific and Arctic during the Late Pleistocene. (*A*) Greenland $\delta^{18}O$ records from NEEM (light blue: ref. 67) and NGRIP (dark blue: ref. 68); (*B*) A $U^{K'}_{37}$ record of SST from ODP1019 (61, 62); (*C*) Global RSL reconstruction, with minimum (dashed line) and maximum (solid line) scenarios (8). Dashed line indicates the Bering sill depth (−53 m); (D) Dates for human presence in North America from archaeological sites south of the ice sheet, with terrestrial sites indicated with tree symbols at the mid-point of start date boundaries (see *SI Appendix*, Table S1 and Dataset S1 for references). Clovis sites are indicated with yellow shading and non-Clovis sites are indicated with dark green shading. Coastal sites are denoted with blue dots. (*E*) Records of alkenone-based $\%C_{37:4}$ as a proxy for sea ice from cores EW0408-85JC (this paper) and U1419 (31) in the Gulf of Alaska. Blue shading denotes values above 5%. (*F*) IRD record from the Gulf of Alaska reflecting major ice-surge events from the Cordilleran (Siku Events: ref. 20; light blue bars). Yellow shaded bars indicate the inter-Siku time intervals in which sea ice was present in the Gulf of Alaska, likely reflecting the most viable windows for the sea-ice highway migration scenario. Pink shaded bars denote the warm climate intervals of the Bølling–Allerød and early Holocene, which were associated with low sea ice and ocean hypoxic events (53–55). The timing of the closure of the interior route is based on (8), whereas the opening is based on (9), however the timing of the closure is less well-constrained than the opening.

have rivaled sustained speeds of even the most skilled Aleut kayakers with efficient skin boats in recent centuries (74). Strategic use of reversing tidal currents and nearshore eddies, along with changing wind conditions, may have partly circumvented the impact of the strong mean-state glacial currents in our model, but such tidal currents are significant primarily in restricted inlets and passages, which were mostly filled with ice during the LGM. Tidal currents in the open ocean are negligible relative to wind-driven and geostrophic currents (75). It remains unclear how effective a barrier stronger glacial currents, especially the Alaska Current, would have been to ancient seafarers moving eastward and southward along the Alaskan coast.

Our simulation with intermediate sea levels (Fig. 2*D*) shows weaker current strengths than either the modern or LGM simulation, suggesting that conditions during the deglacial interval may have been more conducive, or even optimal, for boat transit. This would have been partly contingent on a weakening of the winds during the deglacial period relative to the LGM, which is consistent with dust records (44), although considerable variability in conditions would still prevail amidst these mean-state changes. Expanded area of coastal land due to the retreat of marine-terminating glaciers, warmer climate conditions, and the attenuation of strong ocean currents may have facilitated greater ease of coastal movement and accommodated larger populations, consistent with an increase in evidence for coastal occupation after ~14 ka in British Columbia, Haida Gwaii, Oregon, and the Channel Islands (Figs. 1*D* and 5, ref. 23, and Dataset S1).

Siku Events and Migration on Land. Glacial reconstructions indicate that some unglaciated areas persisted along the Alaskan coast throughout much of the LGM (76, 77), but land area was limited in parts of Southeast Alaska during the local CIS maximum (30). Ice advance from the CIS reached the outer coastal areas near the end of the LGM during brief ~2-kyr advances, ranging regionally between 22 and 16.5 ka (28, 30, 78), although precise locations of the ice edge on the now-submerged continental shelf are not known in detail. The delayed CIS maximum suggests that ice-free coastal areas may have been available along Southeast Alaska's margin before 22 ka, and again after 17 to 16.5 ka, although areas farther south, such as western Vancouver Island, may have been deglaciated earlier (18.5 ka) or remained ice-free throughout the LGM (79).

A dynamic western edge of the CIS is confirmed by IRD deposition indicating repeated advances followed by purges of ice streams from upland Cordilleran ice into the ocean, which would have blocked land-based migration routes. Retreat of marine-terminating ice streams into silled fjord valleys occurred during Siku (iceberg calving) Events (Fig. 3 and refs. 20 and 42). The Siku ice calving intervals probably posed a challenge to navigation on both land and sea. The freshwater flux from Siku ice purges and glacial megafloods were accompanied by extreme cold temperatures (Fig. 3 and refs. 40 and 41) and were likely regional Cordilleran stadials in the North Pacific, which would have been among the most challenging periods for southward dispersal. Nevertheless, rapid melting and ice retreat with warming following Siku Events would have opened up more ice-free coastal areas and possibly led to conditions amenable to human migration. The large iceberg calving events within the plausible time range of coastal migration are Events S1 (~18 to 16.5 ka) and S2 (~27 to 25 ka). A smaller (unnamed) calving interval occurred between ~21 and 22 ka (ref. 20).

Sea-Ice Highway and Winter Dispersals? Gulf of Alaska shorelines had extensive seasonal sea ice during the LGM and early deglaciation, declining substantially only after 14.8 ka (Fig. 3*E*). As this interval now encompasses the most likely time frame identified for the arrival of the first Americans (3, 16–18), it follows that any coastal dispersal during this period would have also required some level of adaptation to sea-ice conditions. Rather than being a barrier to human migration (52), seasonal sea ice could have served as a bridge connecting coastal areas and islands with a relatively traversable surface that doubled as a platform for hunting energy-dense marine mammals. A sea-ice bridge could have connected Siberian and North American land masses earlier than a strictly terrestrial land bridge developed, as well as during the period of shallow land-bridge flooding between ~13 and ~11.5 ka (80).

While we can only speculate on the adaptive strategies of ancient Beringians, people living near the coast during the LGM would have had access to both extensive winter sea ice and ice-free summer conditions, prompting adaptation to a range of conditions, a diverse array of marine resources, and multiple modes of mobility. Modern Inuit communities living in the Arctic rely on sea ice for hunting seals, whales, and polar bears, and refer to a "sea-ice highway" traditionally traversed with the aid of sled dogs (32). Hunting parties can persist on the sea ice for weeks in temporary camps, building snow or ice houses that leave no traces behind. Lunar light and the aurora borealis provide intermittent light sufficient for navigation on a snow or ice-covered landscape or seascape in winter, and moonlight drives phytoplankton productivity and zooplankton migrations even in winter (81, 82), while seals and polar bears are also available from sea ice (83). Although the technological capacities of ancient Beringians would not have been as complex or diverse as the modern Inuit, Upper Paleolithic peoples exposed to sea ice environments for centuries or millennia would likely have developed strategies for effectively exploiting some of the more vulnerable species.

We hypothesize that winter sea-ice conditions in coastal Beringia may have provided a seasonal "sea-ice highway" that offered a platform for winter mobility and a rich source of marine mammals as food to complement boat-based foraging and travel in summer months. A sea-ice highway could have opened coastal migration in the Gulf of Alaska to periods earlier than the deglaciation of the southern coast of Beringia. Forming a contiguous stretch of ecologically familiar resources, Beringian and Gulf of Alaska sea-ice margins may have provided a winter-equivalent of the "kelp highway" (1, 35), creating seasonal continuity in marine resources and facilitating the dispersal of maritime peoples from Northeast Asia to Beringia, and the Pacific Northwest. Transit over shore-fast winter sea ice could help circumvent geographic obstructions such as glaciers and areas of strong north-flowing currents along the outer Alaskan Coast. Winter sea ice would have connected islands in the Beringian Transitory Archipelago and Aleutian Islands, as well as formerly exposed islands on the now-submerged southeast Alaska and British Columbia continental shelf, which would have largely escaped the severe glaciation of the mainland, possibly acting as "stepping stones" for a coastal migration from Beringia into North America (84). In addition to providing a much-needed food source, winter hunting expeditions over sea ice could have scouted out new lands and identified nearby land areas for longer term camps, circumventing perceived barriers to migration.

Although a full test of this hypothesis with local archaeological evidence is challenged by the submergence of coastal areas along the migration pathway, the available genomic and archaeological data points toward a likely migration window between 25 and 16 ka for the first Americans (3, 16–18), which would require not only a coastal route, but dispersals during periods when seasonal sea ice prevailed. Ancient adaptations to sea-ice

environments would have been advantageous for any coastal people living in the subarctic Pacific during the late Pleistocene. Although a previous theory of migration over sea ice in the North Atlantic has been proposed (85), the idea has not been well supported by genomic, archaeological, or oceanographic evidence in that region (86, 87). In contrast, our hypothesis emerges as a natural extension from the available constraints on paleoceanographic conditions and estimated migration time periods in the Northeast Pacific.

Favorable Times for Migration. Optimal conditions for migration would likely require a balance between the presence of shore-fast winter sea ice that connected sufficient coastal land masses, and ice-free summer conditions, along with unglaciated terrestrial refugia. Our data compilation suggests that the most likely time intervals with these conditions were between Siku Events, when winter sea ice was still pervasive, but SSTs were slightly warmer and the climate milder, and ice had retreated off much of the coast into fjords (Fig. 5). Based on the estimated timing of Siku Events (20), available SST records (31, 61–63), and sea-ice reconstructions (our data, refs. 22, 31, 47, and 48), such conditions appear to have occurred between 40 and 32 ka, 29 and 27 ka, 24.5 and 22 ka, 20 and 19 ka, 16.4 and 14.8 ka, and 13 and 11.7 ka (Fig. 5).

Of these possible time periods, the intervals earlier than ~25 ka predate the proposed timing of Beringian–Siberian genetic divergence, so appear unlikely as potential migration periods, at least in the context of existing genomic estimates (16, 17). The 20- to 19-ka window occurs during the estimated maximum of the CIS extent (28, 30), so appears least likely to provide sufficient land refugia along certain portions of the Alaskan coast. However, given the ongoing debates about possible glacial refugia in this region (28–30, 76–79), we cannot rule out this time period as a viable migration window. For now, we highlight this interval as a possibility that requires additional clarity from ice sheet reconstructions and regional sea level and paleoclimate records.

This leaves the intervals 24.5 to 22 ka and 16.4 to 14.8 ka as the most environmentally viable time windows to accommodate early coastal dispersals of humans from Beringia into North America. Conditions likely became more amenable for migration via watercraft during the mid-deglacial, when intermediate sea levels (–75 m) inundated shelves and climate warmed during the Bølling–Allerød (14.7 to 12.9 ka), attenuating coastal currents and exposing more ice-free terrestrial areas along the coast.

These insights from paleoenvironmental records may help focus future efforts to find further evidence for late Pleistocene human occupations around the North Pacific Rim, including archaeological reconnaissance on paleoshorelines and now-submerged islands dating to the most viable time periods for coastal migration. Paleocurrent, climate, and sea-ice reconstructions reveal how climate changes may have facilitated or hindered movement by ancient seafarers in different oceanic regions, which when paired with archaeological and genomic data, may provide insights into coastal dispersals by ancient humans.

Materials and Methods

Ocean Current Simulations. Numerical model simulations were performed using the Massachusetts Institute of Technology General Circulation Model (MITgcm) (88) for the high-resolution ocean current simulations (Fig. 2 and *SI Appendix*, Figs. S1–S4). The model configuration has an eddy-permitting horizontal global grid resolution of 1/6° (~18-km) with 50 levels in the vertical and spacing set from ~10 m in the near-surface to ~450 m at a depth of ~6,000 m. Ocean tracer transport equations are solved using a seventh-order monotonicity preserving advection scheme. There is no explicit horizontal diffusion, and vertical mixing follows the K-Profile Parameterization. The ocean model is coupled to a dynamic-thermodynamic sea-ice model that assumes viscous-plastic ice rheology and computes ice thickness, ice concentration, and snow cover (89).

Numerical experiments were performed using three different boundary conditions to simulate climate during the LGM, Bølling–Allerød, and modern period. LGM simulations were conducted with sea-level 120 m lower than present and with atmospheric boundary conditions (10-m wind, 2-m air temperature, surface humidity, downward longwave and shortwave radiation, precipitation, and runoff) provided by output from the fully coupled Community Climate System Model version 3 (CCSM3) LGM simulation, as described in Condron and Hill (90). Simulations modeling the climate of the Bølling–Allerød are detailed in (91) but, in brief, were performed with sea-level 75 m lower than present (which results in the Bering Strait being closed) and forced with modern (1979 to 2002 monthly mean) atmospheric boundary conditions from the ERA-40 reanalysis data from the European Centre for Medium-range Weather Forecasts. Without access to atmospheric boundary conditions for the specific interval, modern atmospheric conditions provide a reasonable approximation of the relatively warm conditions of the Bølling–Allerød. Modern-day simulations were spun up from ocean salinity and temperature fields provided by the World Ocean Circulation Experiment (WOCE) Hydrographic Program and were forced with atmospheric data from the ECWMF ERA-40 reanalysis.

To simulate the impacts of glacial meltwater input into the Northeast Pacific coastal regions, various fluxes of freshwater, ranging from 0.05 to 3.0 Sv (10^6 m^3 s^{-1}) were released for 1 y in the LGM configuration with a temperature of 0 °C and a salinity of 0 practical salinity units (psu) into the four model grid cells closest to the mouth of the Columbia River. Mean current velocities were integrated between July and December.

To assess the regional climate impact of freshwater input over extended periods of time, such as during Siku Events, additional simulations were run with the low-resolution (~3.75° × 3.75°)-coupled atmosphere-ocean GCM GENMOM (92). Three 300-y simulations were performed using a 17.5-ka configuration: 1) equilibrium control, 2) freshwater flux applied along the Cordilleran ocean margin at a rate of 1-m global sea level equivalent per 500 y, and 3) 2-m global sea level equivalent per 500 y. Model years 200 to 300 are summarized in *SI Appendix*, Figs. S5 and S6.

Sea Ice Reconstructions. Records of the relative abundance of the C_{37} tetra-unsaturated methyl alkenone ($\%C_{37:4}$) are presented for four marine sediment cores in the Gulf of Alaska: EW0408-85JC (59.56°N, 144.15°W, 682 m), EW0408-87JC (58.77°N, 144.50°W, 3,680 m), EW0408-66JC (58.45°N, 137.17°W, 426 m), and EW0408-26JC (57.60°N, 136.72°W, 1,623 m), spanning the last ~18 ka. Elevated concentrations of the tetraunsaturated methyl alkenone have been linked to a specific lineage of alkenones that cooccur with sea ice, making the $\%C_{37:4}$ a proxy for past sea-ice variations (36). Alkenone analyses for the Gulf of Alaska cores were conducted at Oregon State University following the procedures outlined in (54). The $\%C_{37:4}$ is calculated as the abundance ratio of the tetraunsaturated C_{37} ketone to the combined diunsaturated, triunsaturated, and tetraunsaturated C_{37} ketones. Sediments in high-latitude regions show strong correlation between $\%C_{37:4}$ and mean annual sea ice concentrations, with values between 10 and 30% $C_{37:4}$ corresponding to 20 and 40% sea ice concentration in the modern North Pacific (36). Based on this preliminary correlation, we consider $\%C_{37:4}$ values >10% as indicative of the presence of past sea ice during peak cold season months, whereas values of up to 45% $C_{37:4}$ seen in our records likely reflect 50 to 60% mean annual sea ice concentrations, corresponding to ~6 mo of the year. This implies that sea ice would have only persisted during the winter/spring months during the periods of elevated (>10% $C_{37:4}$) values in our records. This is also consistent with the presence of the diunsaturated and triunsaturated alkenones in these same samples, which are used in the $U^{K'}_{37}$ SST index and imply the presence of open ocean coccolithophores, such as *Emiliania huxleyi*.

Age models for these cores are based on previously published radiocarbon chronologies (20, 41), that were recalibrated using the Marine20 calibration curve (93) with the Calib 8.2 software (94), generally following the marine reservoir corrections applied in (41).

North Pacific SST Compilation. Reconstructed SST estimates were compiled that spanned time periods between the LGM (23 to 19 ka) to Holocene time periods, including temperature reconstructions based on the alkenone $U^{K'}_{37}$ index,

Mg/Ca in planktic foraminifera, TEX_{86}, and planktic foraminiferal assemblages, generally following the same criteria, calibrations, and methods in ref. 41. If a site had multiple proxy estimates, SST anomalies were averaged. Additional SST estimates using the BAYSPLINE $U^{K'}_{37}$ calibration (49) are also included in the Dataset S4. Age models were recalibrated using the Marine20 calibration curve (93) with the Calib 8.2 software (94) whenever possible (i.e., when age model data were accessible). In most cases, the most recent age model was adopted, with attempts to retain prior correlation datums (such as tephra or geophysical correlations), along with the recalibrated radiocarbon dates. Generally, the authors' original suggested marine reservoir corrections were used, except in the cases when the original corrections were <550 y, in which case the new default marine reservoir correction of 550 y in Marine20 (93) was used. In some cases, the original age models were retained if there were not sufficient data available to update datasets (i.e., no age model data or depth in core data provided for the SST estimates). Additional information and references for various age models are provided in the supplementary data files (Datasets S2 and S4).

Deglacial SST anomalies for various time slices were calculated for records that had average sample spacing finer than 400 y between 10 and 18 ka. Additional lower resolution sites were included for estimates of LGM-Holocene temperature anomalies. SST anomalies were calculated for the following climate intervals: LGM relative to the early Holocene (23.0 to 19.0 ka − 11.5 to 11.0 ka), Siku Event 1 relative to the LGM (18.0 to 16.5 ka − 23.0 to 19.0 ka), the pre-Bølling period relative to Siku Event 1 (16.4 to 15.0 ka − 18.0 to 16.5 ka), Bølling–Allerød relative to the pre-Bølling period (14.6 to 13.0 ka − 16.4 to 15.0 ka), Younger Dryas relative to Bølling–Allerød (12.7 to 12.0 ka − 14.6 to 13.0 ka), and early Holocene relative to the Younger Dryas (11.5 to 11.0 ka − 12.7 to 12.0 ka). We plot our proxy SST anomalies for the deglacial climate intervals with annual SST estimates from the transient model output of iTRACE (37) (Fig. 4). SST anomalies for the LGM relative to the late Holocene (0 to 3 ka) were also calculated (Dataset S4), but due to few records that extend from the LGM to late Holocene, we opted for the better spatial coverage provided by the LGM-early Holocene anomalies.

An averaged record of high-resolution (~100 y average) Northeast Pacific SST records was also produced, similar to that presented in (41), but the record we present here includes an additional record (a Mg/Ca-based SST reconstruction on the thermocline dwelling *Neogloboquadrina pachyderma sinistral* from core MD02-2496; ref. 63) along with the following $U^{K'}_{37}$ records, which were included in the original average: EW0408-85JC (54), EW0408-66JC & EW0408-26JC (95), JT96-09PC (96), ODP1019 (61, 62), and the Mg/Ca-based SST reconstruction on the planktic species *Globigerina bulloides* from core MD02-2496 (63). All records were linearly interpolated on a 100-y time step and averaged for overlapping time intervals, with a minimum of two records required. As fewer high-resolution records are available beyond 20 ka, the number of records contributing to the stack is reduced going back farther in time, and thus more susceptible to site-specific variability rather than regional trends. An average SST record utilizing two additional, lower resolution $U^{K'}_{37}$ records from the Gulf of Alaska (EW0408-87JC; ref. 41 & U1419; ref. 31) was also produced to increase the number of records in the stack (*SI Appendix*, Fig. S7). For this stack, records were linearly interpolated on a 200-y time step and averaged for overlapping time intervals. A normalized stack was also constructed with all cores on a 200-y time step. Each record was normalized to its mean and SD and then averaged. All versions of the Northeast Pacific stack show similar trends.

Data, Materials, and Software Availability. New data and model results associated with this paper can be found in Supplemental Information or at: https://doi.org/10.5066/P95V8DP2 (97).

ACKNOWLEDGMENTS. We thank K. Brewster, M. Wolhowe, and F. Prahl for assistance with the generation of the $\%C_{37:4}$ records. We thank L. Max, I. Hendy, and N. Harada for assistance with queries regarding SST data and/or age model information for various North Pacific marine sediment cores. We thank C. He, E. Gowan, and O. Romero for providing various datasets, and T. Pico and J. Du for useful discussions. We thank M. Jones for comments on an early version of the manuscript. Finally, we are grateful for the assistance of the reviewers and editors at PNAS. Any use of trade, firm, or product names is for descriptive purposes only and does not imply endorsement by the US Government. Funding was provided by the USGS Climate Research and Development Program, as well as NSF grants 1502754 and 2149564 to A.C.M., NSF grants 1903427 and 2202771 to A.C., and NSF grant 2110923 to B.E.C.

1. J.-M. Erlandson *et al.*, The kelp highway hypothesis: Marine ecology, the coastal migration theory, and the peopling of the Americas. *J. Isl. Coast. Archaeol.* **2**, 161–174 (2007).
2. J.-M. Erlandson, T.-J. Braje, From Asia to the Americas by boat? Paleogeography, paleoecology, and stemmed points of the Northwest Pacific. *Quat. Int.* **239**, 28–37 (2011).
3. T.-J. Braje *et al.*, Finding the first Americans. *Science* **358**, 6363 (2017).
4. B.-A. Potter *et al.*, Early colonization of Beringia and Northern North America: Chronology, routes, and adaptive strategies. *Quat. Int.* **444**, 36–55 (2017).
5. B.-A. Potter *et al.*, Current evidence allows multiple models for the peopling of the Americas. *Sci.Adv.* **4**, eaat5473 (2018).
6. L.-G. Davis, D.-B. Madsen, The coastal migration theory: Formulation and testable hypotheses. *Quat. Sci. Rev.* **249**, 106605 (2020).
7. P.-U. Clark *et al.*, The last glacial maximum. *Science* **325**, 710–714 (2009).
8. E.-J. Gowan *et al.*, A new global ice sheet reconstruction for the past 80,000 years. *Nat. Commun.* **12**, 1199 (2021), 10.1038/s41467-021-21469-w.
9. J. Clark *et al.*, The age of the opening of the Ice-free corridor and implications for the peopling of the Americas. *Proc. Natl. Acad. Sci. U.S.A.* **119**, e2118558119 (2022).
10. L. Becerra-Valdivia, T. Higham, The timing and effects of the earliest human arrivals in North America. *Nature* **584**, 93–97 (2020).
11. D.-L. Jenkins, "Geochronology, archaeological context, and DNA at the Paisley Caves" in *Paleoamerican Odyssey*, K. E. Graf, C. V. Ketron, M. R. Waters, Eds. (Center for the Study of the First Americans, Texas A&M University College Station, 2014), pp. 485–510.
12. M.-R. Waters *et al.*, Pre-clovis projectile points at the Debra L. Friedkin site, Texas–Implications for the late Pleistocene peopling of the Americas. *Sci. Adv.* **4**, eaat4505 (2018).
13. T.-J. Williams, Evidence of an early projectile point technology in North America at the Gault Site, Texas, USA. *Sci. Adv.* **4**, eaar5954 (2018).
14. L. Davis *et al.*, Late upper paleolithic occupation at Cooper's Ferry, Idaho, USA, ~16,000 years ago. *Science* **365**, 891–897 (2019).
15. M.-R. Bennett *et al.*, Evidence of humans in North America during the last glacial maximum. *Science* **373**, 1528–1531 (2021).
16. M. Sikora *et al.*, The population history of northeastern Siberia since the Pleistocene. *Nature* **570**, 182–187 (2019).
17. B. Llamas *et al.*, Ancient mitochondrial DNA provides high-resolution time scale of the peopling of the Americas. *Sci. Adv.* **2**, e1501385 (2016).
18. J.-V. Moreno-Mayer *et al.*, Terminal Pleistocene Alaskan genome reveals first founding population of Native Americans. *Nature* **553**, 203–207 (2018).
19. E. Tamm *et al.*, Beringian standstill and spread of Native American founders. *PLoS One* **2**, e829 (2007).
20. M.-H. Walczak *et al.*, Phasing of millennial-scale climate variability in the Pacific and Atlantic oceans. *Science* **370**, 716–720 (2020).
21. C. Amante, B.-W. Eakins, "ETOPO1 1 Arc-minute global relief model: Procedures, data sources and analysis: NOAA technical memorandum NESDIS NGDC-24" (National Geophysical Data, Center, NOAA, 2009), 10.7289/V5C8276M.
22. M. Méhéust, R. Stein, K. Fahl, R. Gersonde, Sea-ice variability in the subarctic North Pacific and adjacent Bering Sea during the past 25 ka: New insights from IP_{25} and Uk'37 proxy records. *Arktos* **4**, 8 (2018).
23. D. McLaren *et al.*, Late Pleistocene archaeological discovery models on the Pacific Coast of North America. *PaleoAmerica* **6**, 43–63 (2020).
24. J. Clark, J.-X. Mitrovica, J. Alder, Coastal paleogeography of the California–Oregon–Washington and Bering Sea continental shelves during the latest Pleistocene and Holocene: Implications for the archaeological record. *J. Archaeol. Sci.* **52**, 12–23 (2014).
25. T.-C. Royer, B. Finney, An oceanographic perspective on early human migrations to the Americas. *Oceanography* **33**, 32–41 (2020).
26. T.-C. Royer, Baroclinic transport in the Gulf of Alaska: Part II. Fresh water driven Alaska Coastal Current. *J. Marine Res.* **39**, 251–266 (1981).
27. P. Deschamps *et al.*, Ice-sheet collapse and sea-level rise at the Bølling warming 14,600 years ago. *Nature* **483**, 559–564 (2012).
28. A. Lesnek *et al.*, Deglaciation of the Pacific coastal corridor directly preceded the human colonization of the Americas. *Sci. Adv.* **4**, eaar5040 (2018).
29. D. Froese, J.-M. Young, S.-L. Norris, M. Margold, Availability and viability of the ice-free corridor and Pacific coast routes for the peopling of the Americas. *SAA Archaeol. Record* **19**, 27–33 (2019).
30. C.-K. Walcott, J.-P. Briner, J.-F. Baichtal, A.-J. Lesnek, J.-M. Licciardi, Cosmogenic ages indicate no MIS2 refugia in the Alexander Archipelago, Alaska. *Geochronology* **4**, 191–211 (2022).
31. O.-C. Romero *et al.*, Orbital and suborbital variations of productivity and sea surface conditions in the Gulf of Alaska during the past 54,000 years: Impact of iron fertilization by icebergs and meltwater. *Paleoceanogra. Paleoclimatol.* **37**, e2021PA004385 (2022).
32. Inuit Circumpolar Council, The sea ice is our highway: An Inuit perspective on transportation in the Arctic. A contribution to the Arctic marine shipping assessment, 1-27 inuit circumpolar council, Canada (2008). www.inuitcircumpolar.com/project/the-sea-ice-is-our-highway-an-inuit-perspective-on-transportation-in-the-arctic/. Accessed 10 May 2022.
33. V.-D. Steiro *et al.*, Changes in sea ice travel conditions in Uummannaq Fjord, Greenland (1985–2019) assessed through remote sensing and transportation accessibility modeling. *Polar Geogr.* **44**, 282–296 (2021).
34. K. Filbee-Dexter, T. Wernberg, S. Fredriksen, K.-M. Norderhaug, M.-F. Pedersen, Arctic kelp forests: Diversity, resilience, and future. *Glob. Planet. Change* **172**, 1–14 (2019).
35. J.-M. Erlandson, T.-J. Braje, K.-M. Gill, M. Graham, Ecology of the kelp highway: Did marine resources facilitate human dispersal from northeast Asia to the Americas? *J. Island Coastal Archaeol.* **10**, 392–411 (2015).

36. K.-J. Wang *et al.*, Group 2i isochrysidales produce characteristic alkenones reflecting sea ice distribution. *Nat. Commun.* **12**, 15 (2021), 10.1038/s41467-020-20187-z.
37. C. He *et al.*, Abrupt Heinrich Stadial 1 cooling missing in Greenland oxygen isotopes. *Sci. Adv.* **7**, 1–10 (2021).
38. T.-J. Crowley, G.-R. North, *Paleoclimatology* (Oxford, New York, 1991), p. 339.
39. J.-E. O'Connor *et al.*, The Missoula and Bonneville floods–A review of ice-age megafloods in the Columbia River basin. *Earth Sci. Rev.* **208**, 103181 (2020).
40. E. Maier *et al.*, North pacific freshwater events linked to changes in glacial ocean circulation. *Nature* **559**, 241–245 (2018).
41. S.-K. Praetorius *et al.*, The role of Northeast Pacific meltwater events in deglacial climate change. *Sci. Adv.* **6**, eaay2915 (2020).
42. E.-A. Cowan *et al.*, Sediment controls dynamic behavior of a Cordilleran Ice Stream at the last glacial maximum. *Nat. Commun.* **11**, 1826 (2020).
43. A.-M. Balbas *et al.*, ^{10}Be dating of late Pleistocene megafloods and Cordilleran Ice Sheet retreat in the northwestern United States. *Geology* **45**, 583–586 (2017).
44. T. Erhardt *et al.*, Decadal-scale progression of the onset of Dansgaard-Oeschger warming events. *Clim. Past* **15**, 811–825 (2019).
45. J.-A. Barron, D. Bukry, W.-E. Dean, J.-A. Addison, B. Finney, Paleoceanography of the Gulf of Alaska during the past 15,000 years: Results from diatoms, silicoflagellates, and geochemistry. *Marine Micropaleontol.* **72**, 176–195 (2009).
46. B.-E. Caissie *et al.*, Last Glacial Maximum to Holocene sea surface conditions at Umnak Plateau, Bering Sea, as inferred from diatom, alkenone, and stable isotope records. *Paleoceanography* **25**, PA1206 (2010).
47. A. de Vernal, T.-F. Pedersen, Micropaleontology and palynology of core PAR87A-10: A 23,000-year record of paleoenvironmental changes in the Gulf of Alaska, northeast North Pacific. *Paleoceanography* **12**, 821–830 (1997).
48. N. Harada *et al.*, Sea surface temperature changes in the Okhotsk Sea and adjacent North Pacific during the last glacial maximum and deglaciation. *Deep Sea Res. II Top. Stud. Ocenogr.* **61–64**, 93–105 (2012).
49. J.-E. Tierney, M.-P. Tingley, BAYSPLINE: A new calibration for the alkenone paleothermometer. *Paleoceanography* **33**, 281–301 (2018).
50. N. Misarti *et al.*, Early retreat of the Alaskan Peninsula Glacier complex and the implications for coastal migration of first Americans. *Quat. Sci. Rev.* **48**, 1–6 (2012).
51. D.-M. Peteet, D.-H. Mann, Late-glacial vegetational, tephra, and climatic history of southwestern Kodiak Island. Alaska. *Écoscience* **1**, 255–267 (1994).
52. T.-A. Ager, Late Quaternary vegetation development following deglaciation of Northwestern Alexander Archipelago, Alaska. *Front. Earth Sci.* **7**, 104 (2019).
53. M.-H. Davies *et al.*, The deglacial transition on the southeastern Alaska Margin: Meltwater input, sea level rise, marine productivity, and sedimentary anoxia. *Paleoceanography* **26**, PA2223 (2011).
54. S.-K. Praetorius *et al.*, North Pacific deglacial hypoxic events linked to abrupt ocean warming. *Nature* **527**, 362–366 (2015).
55. S.-E. Moffitt *et al.*, Paleoceanographic Insights on recent oxygen minimum zone expansion: Lessons for modern oceanography. *PLoS One* **10**, e0115246 (2015).
56. J.-W.-B. Rae *et al.*, Overturning circulation, nutrient limitation, and warming in the Glacial North Pacific. *Sci. Adv.* **6**, eabd1654 (2020).
57. J. Kurek *et al.*, Late Quaternary paleoclimate of western Alaska inferred from fossil chironomids and its relation to vegetation histories. *Quat. Sci. Rev.* **28**, 799–811 (2009).
58. S.-A. Elias, B. Crocker, The Bering Land Bridge: A moisture barrier to the dispersal of steppe-tundra biota? *Quat. Sci. Rev.* **27**, 2473–2483 (2008).
59. M. Löfverström, J. Liakka, On the limited ice intrusion in Alaska at the LGM. *GRL* **43**, 11030–11038 (2016).
60. J.-E. Tierney *et al.*, Glacial cooling and climate sensitivity revisited. *Nature* **584**, 569–573 (2020).
61. J.-A. Barron, L. Heusser, T. Herbert, M. Lyle, High-resolution climatic evolution of coastal northern California during the past 16,000 years. *Paleoceanography* **18**, 1020 (2003).
62. T.-D. Herbert, "Alkenone paleotemperature determinations" in *Treatise on Geochemistry*, H. Elderfield, H. D. Holland, K.-A. Barron, K. K. Turekian, Eds. (Elsevier, 2003), pp. 391–432.
63. M.-A. Taylor, I.-L. Hendy, D.-K. Pak, Deglacial ocean warming and marine margin retreat of the Cordilleran Ice Sheet in the North Pacific Ocean. *Earth Planet. Sci. Lett.* **403**, 89–98 (2014).
64. R. Vachula *et al.*, Evidence of Ice Age humans in eastern Beringia suggests early migration to North America. *Quat. Sci. Rev.* **205**, 35–44 (2019).
65. B.-A. Potter *et al.*, Current understanding of the earliest human occupations in the Americas: Evaluation of Becerra-Valdivia and Higham (2020). *PaleoAmerica* **8**, 62–76 (2022).
66. T. Goebel, J.-F. Hoffecker, K.-E. Graf, R.-S. Vachula, Archaeological reconnaissance at Lake E5 in the Brooks Range, Alaska and implications for the early human biomarker record of Beringia. *Quat. Sci. Rev.* **286**, 107553 (2022).
67. C. Buizert *et al.*, Greenland temperature response to climate forcing during the last deglaciation. *Science* **345**, 1177–1180 (2014).
68. S.-O. Rasmussen *et al.*, A stratigraphic framework for abrupt climatic changes during the Last Glacial period based on three synchronized Greenland ice-core records: Refining and extending the INTIMATE event stratigraphy. *Quat. Sci. Rev.* **106**, 14–28 (2014).
69. C.-F. Ardelean *et al.*, Evidence of human occupation in Mexico around the Last Glacial Maximum. *Nature* **584**, 87–92 (2020).
70. C.-G. Oviatt, D.-B. Madsen, D. Rhode, L.-G. Davis, A critical assessment of claims that human footprints in the Lake Otero basin, New Mexico date to the Last Glacial Maximum. *Quat. Res.* 1–10 (2022).
71. T.-A. Surovell *et al.*, Late date of human arrival to North America: Continental scale differences in stratigraphic integrity of pre-13,000 BP archaeological sites. *PLoS One* **17**, e0264092 (2022).
72. B. Fitzhugh, "The Paleolithic of Maritime Northeast Asia and the Search for Maritime Beringians" in *Maritime Prehistory of Northeast Asia*, J. Cassidy *et al.*, Eds. (2022), pp. 349–378.
73. M. Fujita *et al.*, Advanced maritime adaptation in the western Pacific coastal region extends back to 35000–30000 years before present. *Proc. Natl. Acad. Sci. U.S.A.* **113**, 11184–11189 (2016).
74. G.-B. Dyson, The Aleutian Kayak. *Sci. Am.* **282**, 84–91 (2000).
75. D. Stammer *et al.*, Accuracy assessment of global barotropic ocean tide models. *Rev. Geophys.* **52**, 243–282 (2014).
76. T.-H. Heaton, S.-L. Talbot, G.-F. Shields, An ice age refugium for large mammals in the Alexander Archipelago, southeastern Alaska. *Quat. Res.* **46**, 186–192 (1996), 10.1006/qres.1996.0058.
77. P.-E. Carrara, T.-A. Ager, J.-F. Baichtal, Possible refugia in the Alexander Archipelago of southeastern Alaska during the late Wisconsin glaciation. *Can. J. Earth Sci.* **44**, 229–244 (2007).
78. C.-M. Darvill *et al.*, Retreat of the western Cordilleran ice sheet margin during the last deglaciation. *Geophys. Res. Lett.* **45**, 9710–9720 (2018).
79. C.-F.G. Hebda *et al.*, Late Pleistocene paleoenvironments and a possible glacial refugium on northern Vancouver Island, Canada: Evidence for the viability of early human settlement on the northwest coast of North America. *Quat. Sci. Rev.* **279**, 107388 (2022).
80. T. Pico, J.-X. Mitrovica, A.-C. Mix, Sea level fingerprinting of the Bering Strait flooding history detects the source of the Younger Dryas climate event. *Sci. Adv.* **6**, eaay2935 (2020).
81. A. Randelhoff *et al.*, Arctic mid-winter phytoplankton growth revealed by autonomous profilers. *Sci. Adv.* **6**, eabc2678 (2020).
82. K.-S. Last, L. Hobbs, J. Berge, A.-S. Brierley, F. Cottier, Moonlight drives ocean-scale mass vertical migration of zooplankton during the Arctic winter. *Curr. Biol.* **26**, 244–251 (2016).
83. T.-W. Bentzen *et al.*, Variation in winter diet of southern Beaufort Sea polar bears inferred from stable isotope analysis. *Can. J. Zool.* **85**, 596–608 (2007).
84. J. Dobson, G. Spada, G. Galassi, The Bering Transitory Archipelago: Stepping stones for the first Americans. *C. R. Geosci.* **353**, 55–65 (2021).
85. B. Bradley, D. Stanford, The North Atlantic ice-edge corridor: A possible palaeolithic route to the new world. *World Archaeol.* **36**, 459–478 (2004).
86. K. Westley, J. Dix, The Solutrean Atlantic hypothesis: A view from the ocean. *J. North Atlantic* **1**, 85–98 (2008).
87. M.-J. O'Brien *et al.*, On thin ice: Problems with the Stanford and Bradley's proposed Solutrean colonization of North America. *Antiquity Publications* **88**, 606–624 (2014).
88. J. Marshall, A. Adcroft, C. Hill, L. Perelman, C. Heisey, A finite-volume, incompressible Navier Stokes model for studies of the ocean on parallel computers. *J. Geophys. Res. Oceans* **102**, 5753–5766 (1997).
89. M. Losch, D. Menemenlis, J.-M. Campin, P. Heimbach, C. Hill, On the formulation of sea-ice models. Part 1: Effects of different solver implementations and parameterizations. *Ocean Model.* **33**, 129–144 (2010).
90. A. Condron, J.-C. Hill, Timing of iceberg scours and massive ice-rafting events in the subtropical North Atlantic. *Nat. Commun.* **12**, 1–14 (2021).
91. S. Pendleton, A. Condron, J. Donnelly, The potential of Hudson valley glacial floods to drive abrupt climate change. *Commun. Earth Environ.* **2**, 1–7 (2021).
92. J.-R. Alder, S.-W. Hostetler, Global climate simulations at 3000-year intervals for the last 21 000 years with the GENMOM coupled atmosphere-ocean model. *Clim. Past* **11**, 449–471 (2015).
93. T.-J. Heaton *et al.*, Marine20–the marine radiocarbon age calibration curve (0–55,000 Cal BP). *Radiocarbon* **62**, 779–820 (2020).
94. M. Stuiver, P.-J. Reimer, R.-W. Reimer, CALIB 8.2 [WWW program] (2021). http://calib.org. accessed May 2022.
95. S.-K. Praetorius *et al.*, Interaction between climate, volcanism, and isostatic rebound in Southeast Alaska during the last deglaciation. *Earth Planet. Sci. Lett.* **452**, 79–89 (2016).
96. S.-S. Kienast, J.-L. McKay, Sea surface temperatures in the subarctic northeast Pacific reflect millennial-scale climate oscillations during the last 16 kyrs. *Geophys. Res. Lett.* **28**, 1563–1566 (2001).
97. J. R. Alder, S. K. Praetorius, A. Condron, Data release for Ice and ocean constraints on early human migrations into North America along the Pacific coast, https://doi.org/10.5066/P95V8DP2